LANGMUIR Article
Cite This: Langmuir XXXX, XXX, XXX−XXX
pubs.acs.org/Langmuir

# Role of Surfactant in Evaporation and Deposition of Bisolvent Biopolymer Droplets

Dong-Ook Kim, Arif Rokoni, Paul Kaneelil, Chunxiao Cui, Li-Hsin Han, and Ying Sun*

Department of Mechanical Engineering and Mechanics, Drexel University, Philadelphia, Pennsylvania 19104, United States

**ABSTRACT:** Inkjet printing of biopolymer droplets is gaining popularity because of its potential applications in regenerative medicine, particularly the fabrication of tissue-regenerative scaffolds. The quality of bioprinting, which affects cellular behaviors and the subsequent tissue formation, is determined by the solvent evaporation and deposition processes of biopolymer droplets, during which instantaneous local viscosity and surface tension changes occur because of the redistribution of the biopolymer inside the drop. Such dynamics is complex and not well understood. Most biopolymer inks also contain multiple solvents of distinct evaporation rates, further complicating the system dynamics. Using high-speed interferometry, we directly observe in real time the instantaneous drop shape of inkjet-printed picoliter gelatin drops containing glycerol and water. It is observed that, for bisolvent gelatin drops with surfactants, highly viscous gelatin and glycerol accumulated near the pinned contact line at an early stage suppress the evaporation-driven outward flow and create a stagnation zone near the contact line region. Lower surface tension at the contact line, because of its high local surfactant concentration, as compared to the drop apex induces a strong Marangoni recirculation, which in conjunction with a stagnation zone in the contact line region causes the instantaneous drop shape to transition from a spherical cap to a volcano shape during evaporation and resulting in a volcano-like deposition profile. In contrast, the suppressed evaporation outward flow together with a weak Marangoni flow leads to a domelike deposition for the case without surfactant. The role of surfactant in polymer drop deposition with water-only solvent is also investigated and compared against that of bisolvent drops. For the single-solvent case, the deposition profile is found to shift from a coffee-eye shape in the presence of surfactant to a uniform deposition without surfactant. The results reveal new insight into the complex role surfactant plays during polymer drop evaporation and deposition processes.

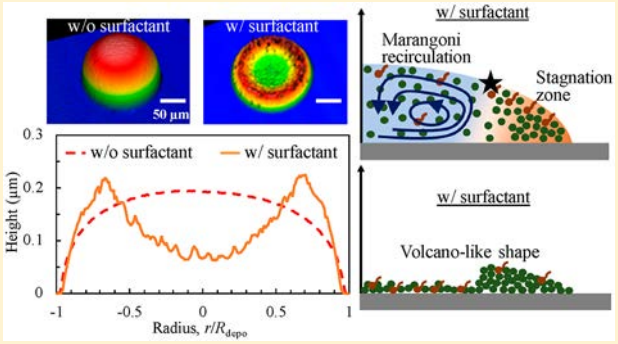


## INTRODUCTION

Growing markets in organic microdevices call for advanced technologies to facilitate the control and assembly of natural and synthetic polymers. Established devices include organic light-emitting diodes (OLEDs),[1] organic solar cells,[2] and more recently biomedical implants for healing or controlling wounds and diseases.[3−5] Such development has motivated intensive studies for creating better strategies for polymer manipulation, including methods for delivering polymers by microscopic volumes, assembling the volumes with a micrometer- or submicrometer-size resolution, and subsequently fusing them into a functional device. Among all, inkjet printing,[6,7] which delivers picoliter-sized inks in a drop-on-demand manner, offers advantages of low cost, micrometer-scale resolution, high speed, and most importantly, the flexibility that allows various organic and inorganic compounds to be selected and assembled. This makes inkjet printing particularly suitable for biomedical applications, as it may rapidly form biomimetic constructs consisting of various biological cells and biopolymers including polysaccharides and proteins.[8−10] These constructs are being applied as models for disease research as well as artificial tissues for implants[11,12] including artificial blood vessels,[13] skin, and cartilage.[14]

A successful inkjet-printing practice demands precise control of the droplet deposition profile since the individual droplet shape determines the device's geometric resolution and thus impacts the device functionalities. Polymer inks often contain a mixture of polymers and solvents. During the drop deposition process, the ink composition changes and the droplet shape evolves as the solvents evaporate and perform microflows and solutes simultaneously self-assemble, precipitate, and even chemically react. To decipher such dynamics, experimental studies[1,10,15−19] and numerical simulations[20−22] have been conducted to examine the complex interplay of solvent evaporation, substrate properties, and environment conditions to better control the final deposition morphologies. For example, Cui et al.[23] and Seo et al.[24] showed that the polymers in aqueous drops suppressed the coffee-ring effect and led to uniform depositions. Baldwin et al.[10] examined the drying of polymer sessile drops by changing relative humidity, temperature, pressure, droplet volume, and initial contact angle and found that the deposition profile is dictated only by polymer

Received: June 5, 2019
Revised: August 23, 2019
Published: September 9, 2019






DOI: 10.1021/acs.langmuir.9b01705
Langmuir XXXX, XXX, XXX−XXX

concentration and the relative effects of evaporation and diffusion. Kajiya et al.[25] observed the effect of contact line pinning on the deposition profile where the volcano-like deposition was found as a result of the long pinning time and a highly viscous region close to the contact line, while the polymer-induced Marangoni flow toward the drop center aided contact line depinning and led to a uniform deposition. A combined numerical and experimental study was conducted by Eales et al.[20] in which the lubrication theory is used to obtain the instantaneous height profile and polymer volume fraction of an evaporating drop, and the viscosity increase with polymer concentration is considered while a gelled region forms near the contact line, minimizing the evaporation. For a polymer drop with a single solvent, increasing the initial polymer concentration transitions the deposition profile from ringlike to more uniform. However, for a bisolvent polymer drop, the evaporation ratio between the two solvents plays an important role in the final deposition,[26,27] where the solvental Marangoni flow induced by a mixture of low boiling point/high surface tension solvent and high boiling point/low surface tension solvent leads to a domelike deposition.[28] Soltman and Subramanian[1] and Kim et al.[29] showed that increasing the substrate temperature of polymer droplets enhances the ring formation because of the strong evaporation-driven flow to the contact line, where the thermal Marangoni flow is found to be negligible.

The surfactant-driven Marangoni flow adds a new dimension to the polymer drop evaporation process. Kajiya et al.[30] obtained more uniform deposition when a small amount of surfactant was added to a polymer drop, inducing a surfactant Marangoni flow[24,31] as the concentration of the surfactant increases near the contact line. However, a nonuniform volcano-like polymer deposition with surfactants was reported for small drops and low initial polymer concentrations.[32] Similar volcano-like deposition with surfactant is also observed in bisolvent polymer drops in our experiments, while a domelike deposition is observed for the same drops without surfactant. Because of these contradictory observations, the effects of surfactant on the evaporation and microflows inside the polymer drop leading to the final deposition profile need to be better understood. In particular, how the competition between the evaporation-driven outward flow and Marangoni flow in the presence of surfactant affects the deposition has not been fully explored for complex polymer drops.

In this study, we aim to understand the effect of surfactant on final deposition morphologies of inkjet-printed, picoliter bisolvent drops containing a biopolymer, via in situ observation of the drop evaporation process. The biopolymer used for this study was chemically modified gelatin, a protein that is often used for making tissue-engineering implants.[5,11] The gelatin was introduced with extra carboxylic function groups (gel-COOH hereinafter) to enhance gelatin's solubility and optimize jetting and printing properties. High-speed interferometry was used to obtain the instantaneous drop shape. Microflows inside the drop was visualized using fluorescence microscopy with low-concentration tracer particles. The postmortem deposition profile was analyzed by optical profilometry. We report that the Marangoni recirculation with a stagnation zone near the contact line dictates the role of surfactant in the deposition of inkjet-printed bisolvent polymer drops, resulting in a volcano-like profile. In contrast, the suppressed evaporation-driven outward flow in conjunction with a weak Marangoni flow leads to a domelike deposition for the case of bisolvent polymer drops without surfactant. For polymer drops with water-only solvent, continuous contact line depinning is observed both with and without surfactant in the absence of a stagnation zone. The role of surfactant is found to cause the deposition profile to undergo a transition from coffee-eye-like (i.e., a central deposition with a thin outer ring) with surfactant to a uniform deposition without surfactant.

## EXPERIMENTAL METHODS

A custom-built printing setup consisting of a piezoelectric drop-on-demand printer synchronized with side-view flash photography to ensure stable droplets from a printhead with an orifice diameter of 60 $\mu$m (MicroFab MJ-AL-01, Plano, TX) is shown in Figure 1a. The

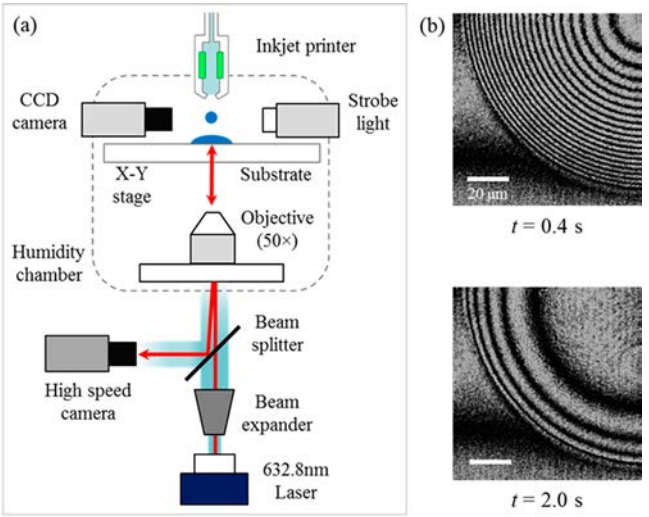


**Figure 1.** (a) Schematic depiction of the interferometry setup for inkjet-printed evaporating drops. The dashed line represents the humidity-controlled chamber. (b) Interferometry images of an evaporating aqueous polymer drop of 113 pL on a plasma-cleaned glass substrate containing 3 wt % gel-COOH, 12 wt % glycerol, and water at $t$ = 0.4 s and $t$ = 2.0 s after deposition. The relative humidity of the chamber is 35%. The scale bars represent 20 $\mu$m.

picoliter-sized droplets were formed via a pneumatic control device (MicroFab) and a waveform generator (JetDrive). The side-view imaging of the drop was conducted using a 12× Navitar lens (Rochester, NY) on a SensiCam CCD camera (Germany) in tandem with a halogen strobe light (PerkinElmer, Waltham, MA). The lighting, imaging, and droplet jetting were synchronized with a delay generator (SRS DG645, Sunnyvale, CA) to obtain droplets of ≈60 $\mu$m diameter. The droplets were printed onto cleaned glass slides (Chemglass, Vineland, NJ), which were also made more hydrophilic by plasma cleaning (2 min of air plasma at 18 W and 250 mTorr, Harrick Plasma PDC-32G, Ithaca, NY). All the experiments were performed within 5 min of plasma cleaning. The relative humidity was controlled using an environmental chamber and the ambient temperature was maintained at 22 °C.

The bottom-view interferometry imaging was conducted on the basis of constructive (bright fringes) and destructive (dark fringes) interference resulting from the phase shift between the incident light reflected from the drop−air interface and the glass substrate. The interferometry imaging setup consists of a 50× objective connected to an inverted microscope (Zeiss Axio Observer A1) illuminated by a 632.8 nm helium−neon laser (Thorlabs HNL225R, beam diameter 0.7 mm, Newton, NJ) expanded through a beam expander (Thorlabs GBE20-A). The interferometry images were recorded at 2000 frames/s with a resolution of 0.4 × 0.4 $\mu$m/pixel by a high-speed camera (Phantom V711, Wayne, NJ). The captured images (Figure 1b) were analyzed on the basis of the well-known premise that the fringe-to-


DOI: 10.1021/acs.langmuir.9b01705
Langmuir XXXX, XXX, XXX−XXX

fringe spacing correlates to a local drop thickness differential of $\lambda/2$, where $\lambda$ is the wavelength of the light source.[33,34] The maximum measurable thickness depends on the coherence of the light source and is over 10 $\mu$m in our experiments. The minimum measurable thickness depends on the wavelength of the light source and is $\lambda/4 \approx$ 158.2 nm in the present study. With a temporal resolution of 500 $\mu$s, the interferometry technique allows for the instantaneous measurement of the local drop thickness, from which the drop profile is determined using the cubic spline interpolation function of MATLAB.[35] The volume of the drop was then calculated from the drop profile using Pappus's centroid theorem.[36] All deposited samples were stored at an ambient temperature of 22 °C and a relative humidity of 35% for over 48 h to ensure that evaporation was complete. The deposition profile was then determined using an optical profilometer (Zygo 7100, Middlefield, CT) which has a lateral resolution of 0.4 $\mu$m and a vertical resolution of 0.1 nm. The deposition profile was remeasured after a week to ensure it remained the same.

The carboxylated gelatin (gel-COOH) was made from the gelatin solution which was prepared by dissolving 10 g of powdered gelatin from a cold-water fish skin (Sigma-Aldrich G7041) into 100 mL of deionized water in a conical flask heated at 75 °C under continuous stirring for 20 min. The gelatin solution was filtered using a 0.22 $\mu$m syringe filter. Two solutions, one made of 0.25 g of succinic acid (SA) in 10 mL of acetone and another with 0.4 g of sodium hydroxide in 8 mL of deionized water, were prepared for synthesis of gel-COOH. The synthesis process started with adding the sodium hydroxide buffer solution into the gelatin solution to reach a pH value of 7. A 0.3 mL sodium hydroxide buffer solution and a 1.0 mL SA solution were then added into the gelatin solution and the process was repeated until the SA solution was depleted, keeping the mixture at the pH value of 7. After the mixture was stirred at room temperature for at least 3 h, the gel-COOH was then purified several times with a dialysis process in deionized water, freeze-dried, and stored at −20 °C before use. For inkjet-printing experiments, the gel-COOH ink was prepared by dissolving 3 wt % gel-COOH into deionized water and glycerol (Acros Organics), and with or without 0.75 wt % Surfynol 440 surfactant (Air Products and Chemicals), a nonionic and nonfoaming surfactant.[37] The physical properties of the solvents and surfactant in the ink solution at room temperature are summarized in Table 1.

**Table 1. Properties of Solvents and the Surfactant in the Ink Solution at 295 K**

| name | viscosity (mPa·s) | surface tension (mN/m) | boiling point (K) |
|---|---|---|---|
| glycerol | 830 ± 20 | 63.1 ± 2 | 563.2[38] |
| water | 0.89 ± 0.03 | 72 ± 2 | 373.2[39] |
| Surfynol 440 | 150[37] | | |

Figure 2a shows the change of viscosity, $\eta$, as a function of the concentration of all nonwater contents in gel-COOH−water, glycerol−water, and gel-COOH−glycerol−water solutions measured using a viscometer (Brookfield DV-II+Pro). The viscosity of the gel-COOH−water mixture (black square) increases about 39 times as the concentration of gel-COOH in water increases from 3 to 20 wt %, while the increase is about 709 times for the glycerol−water mixture (blue circle) as the glycerol concentration changes from 10 to 100 wt %. On the other hand, the viscosity of the gel-COOH−glycerol−water solution (red diamond) increases from 0.003 to 0.308 Pa·s as the concentration of gel-COOH and glycerol in water increases from 15 to 65 wt %, while keeping the gel-COOH/glycerol ratio fixed at 1:4. Figure 2b shows the surface tension variation for different nonwater content concentrations measured by a tensiometer (Attension Sigma 701). The surface tension of the glycerol−water mixture decreases from 71 to 63 mN/m when the glycerol concentration increases from 0 to 100 wt %. Increasing gel-COOH concentration from 3 to 20 wt % reduces the surface tension of gel-COOH−water mixture from 49 to 36 mN/m. In addition, adding a small amount (e.g., 0.75 wt %) of surfactant in water significantly reduces the water surface tension from 72 to 29 mN/m.

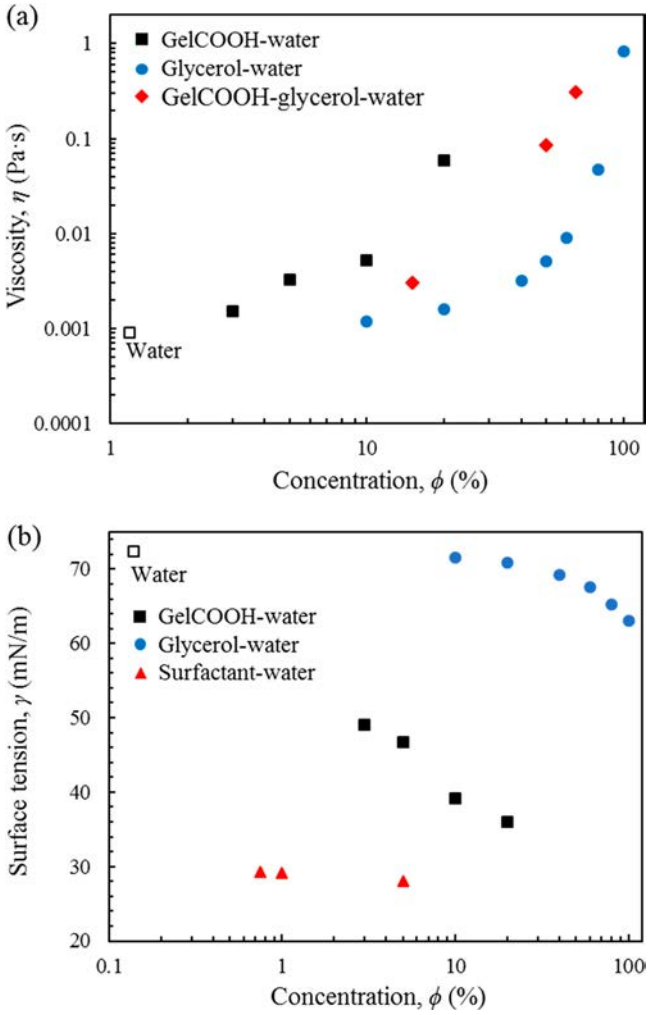


**Figure 2.** Properties of ink solutions as a function of the nonwater concentration, $\phi$. (a) Viscosity ($\eta$) of gel-COOH−water (black square), glycerol−water (blue circle), and gel-COOH−glycerol−water (red diamond, with gel-COOH/glycerol = 1:4) solutions. (b) Surface tension ($\gamma$) of gel-COOH−water (black square), glycerol−water (blue circle), and surfactant−water (red triangle) solutions. The viscosity and surface tension of pure water are plotted as hollow squares for reference.

## RESULTS AND DISCUSSION

To understand the dependence of deposition morphologies on surfactant, Figure 3 shows the deposition profiles of inkjet-printed drops containing 3 wt % gel-COOH in 12 wt % glycerol−water without (Figure 3a) and with 0.75 wt % surfactant (Figure 3b), as well as in 6 wt % glycerol−water without (Figure 3c) and with surfactant (Figure 3d), on a plasma-cleaned glass substrate with an in-flight drop diameter of 60 $\mu$m. The corresponding centerline height profiles without and with surfactant for the 12 and 6 wt % glycerol cases are shown in Figure 3e,f, respectively. For both 12 and 6 wt % glycerol cases, the deposition profiles of the glycerol−water bisolvent polymer droplets with surfactant show volcano-like profiles (Figure 3b,d), which are very different from the domelike depositions without surfactant (Figure 3a,c). In contrast to adding surfactant as a means to increase the


DOI: 10.1021/acs.langmuir.9b01705
Langmuir XXXX, XXX, XXX−XXX

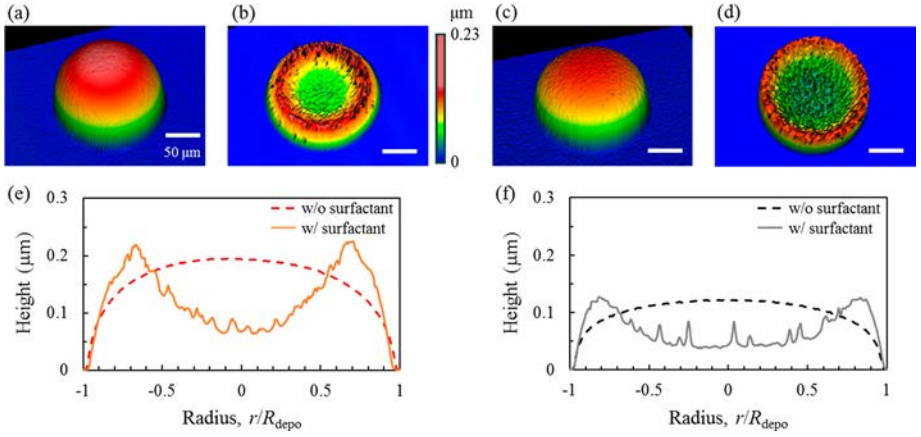


**Figure 3.** Deposition profiles of inkjet-printed polymer droplets with 3 wt % gel-COOH in 12 wt % glycerol−water (a) without and (b) with surfactant, and in 6 wt % glycerol−water (c) without and (d) with surfactant on a plasma-cleaned glass. Centerline height profiles of the final deposition containing 3 wt % gel-COOH in (e) 12 wt % glycerol−water without and with surfactant and in (f) 6 wt % glycerol−water without and with surfactant. The in-flight drop diameter is 60 $\mu$m at a relative humidity of 35%. The droplet deposition radius, $R_{depo}$, is ≈170 $\mu$m in all cases of Figure 3. The scale bar represents 50 $\mu$m.

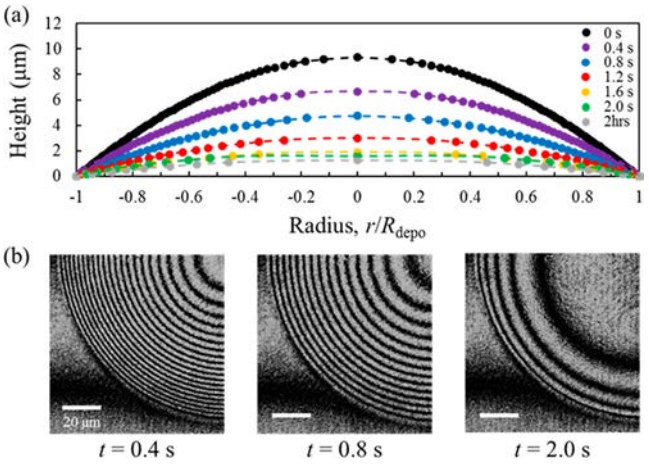


**Figure 4.** (a) Instantaneous drop shapes every 0.4 s for the first 2 s and in 2 h without surfactant based on interferometry and (b) interferometry images of inkjet-printed evaporating aqueous polymer droplets on a plasma-cleaned glass substrate containing 3 wt % gel-COOH, 12 wt % glycerol, and 85 wt % water at $t$ = 0.4, 0.8, and 2.0 s. The experimental conditions are the same as those in Figure 3. The scale bar represents 20 $\mu$m.

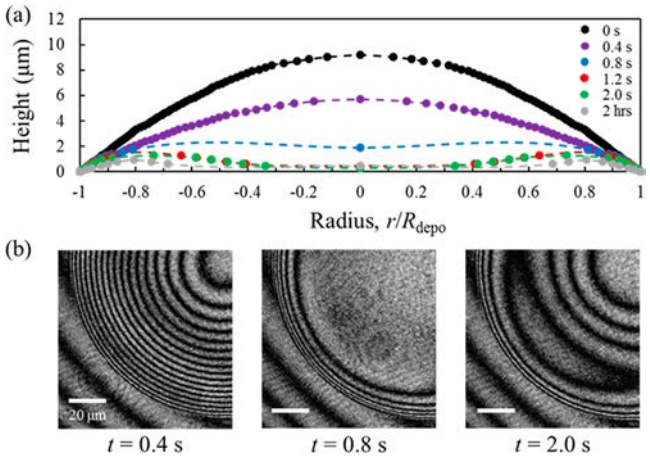


**Figure 5.** (a) Instantaneous drop shapes with surfactant based on interferometry showing the inflection point starting at $t$ = 1.2 s and (b) interferometry images of inkjet-printed evaporating aqueous polymer droplets on a plasma-cleaned glass substrate containing 3 wt % gel-COOH, 12 wt % glycerol, 0.75 wt % surfactant, and water at $t$ = 0.4, 0.8, and 2.0 s. The experimental conditions are the same as those in Figure 3. The scale bar represents 20 $\mu$m.

uniformity of the final deposition of picoliter polymer drops,[30,32] uniform deposition is not observed with surfactant in this study. Moreover, as the concentration of glycerol increases in the gel-COOH−glycerol−surfactant−water drops shown in Figure 3b,d, the distance between the contact line edge and the deposition peak increases. In the absence of surfactant, however, a domelike deposition profile is observed at different glycerol concentrations, as shown in Figure 3a,c. Eales et al.[26] has also predicted a domelike deposition profile for the bisolvent case when the relative volatility, that is, the evaporation rate ratio between the more volatile and less volatile solvent, reaches about 50. When the relative volatility of the bisolvent is high, such as glycerol and water in the current study, the contact line region becomes rich in the less volatile component (glycerol) but lean in the more volatile liquid (water), which in turn suppresses the evaporation flux at the contact line, hinders the coffee-ring effect, and results in a domelike deposition as shown in Figure 3a,c.

Figure 4a shows the instantaneous drop shapes every 0.4 s without surfactant based on in situ interferometry of an evaporating droplet containing 3 wt % gel-COOH in 12 wt % glycerol and 85 wt % water, the same case considered in Figure 3a, providing a better understanding of the deposition profile with and without surfactant. The drop maintains a domelike shape and the contact line is pinned during the entire evaporation process. The drop height decreases faster at an early stage of evaporation and slows down as water is gradually depleted. Within 2.0 s, 80% of the drop volume evaporates, which is much longer than the pure water drops of the same size with a total evaporation time of about 0.79 s.[40] Here, the total evaporation time of a pure water drop is estimated assuming diffusion-limited evaporation of a spherical cap drop with a pinned contact line following $t_f = \pi\rho R_{depo}^2 \tan(\Theta/2)/[8D(1 - RH)c_v]$,[41,42] where $D$ is the diffusivity of water vapor in air, $c_v$ is the saturated vapor concentration, RH is the relative humidity, $\Theta$ is the apparent contact angle of the droplet, $R_{depo}$



DOI: 10.1021/acs.langmuir.9b01705
Langmuir XXXX, XXX, XXX−XXX

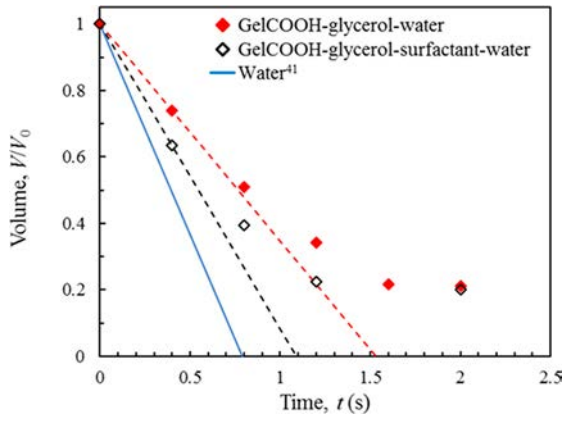


**Figure 6.** Comparison of normalized drop volumes, $V/V_0$, versus time with and without surfactant for droplets containing 3 wt % gel-COOH, 12 wt % glycerol, and 85 wt % water on a plasma-cleaned glass substrate. The experimental conditions are the same as those in Figures 3a,b. The dashed lines assume linear drop volume decrease with time as in a pure water drop on a hydrophilic surface. The solid blue line shows pure water of the same size.[41]

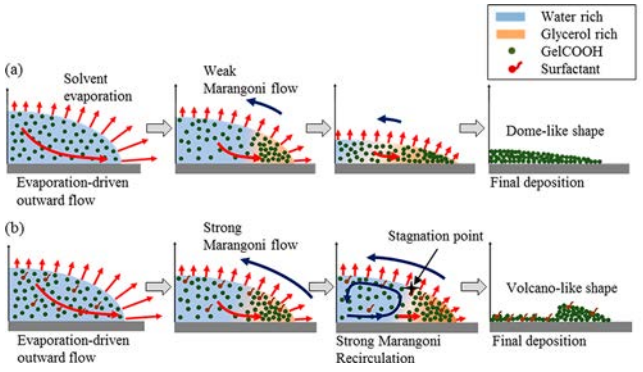


**Figure 7.** Schematics of the drop evaporation and polymer deposition process of a gel-COOH−glycerol−water droplet (a) without and (b) with surfactant. A highly viscous stagnation zone near the contact line is formed for both cases because of the accumulation of gel-COOH and glycerol. The strong Marangoni recirculation induced by surfactant in conjunction with the stagnation zone leads to a volcano-like deposition pattern with surfactant.

$= \{\pi d_0^3/[3\pi \tan(\Theta/2)]\}^{1/3}$ is the droplet deposition radius, and $d_0$ is the drop in-flight diameter. This longer evaporation time for the bisolvent polymer drop confirms that as water evaporates, the accumulation of gel-COOH and glycerol at the pinned contact line reduces the evaporation flux near the contact line and suppresses the evaporation-driven outward flow as compared to that of a pure water drop. After 2.0 s, evaporation slows down and the drop volume reduces from 20% to 14.9% in 2 h. Interferometry images shown in Figure 4b reveal the changes in fringe spacing over time. The fringe spacing, corresponding to drop height variation, is small at an early time, for example, $t$ = 0.4 s, and increases when $t$ = 0.8 s. At $t$ = 2.0 s, no fringe is seen at the drop center, indicating no height variation or a flat drop profile.

Figure 5a shows the changes in drop shape every 0.4 s with surfactant based on interferometry for the same case considered in Figure 3b. The contact line is pinned during the entire evaporation process and the drop initially maintains a domelike shape at $t$ = 0.4 s, similar to that without surfactant shown in Figure 4a. The drop shape then starts to change from

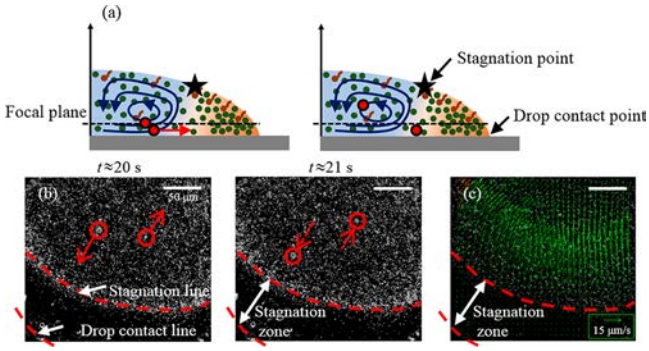


**Figure 8.** (a) Schematic of microflows inside a drop consisting of 3 wt % gel-COOH−12 wt % glycerol−0.75 wt % surfactant−water. The accumulation of gel-COOH, glycerol, and surfactant near the contact line creates a highly viscous stagnation zone. The surfactant-driven Marangoni flow in conjunction with the stagnation zone leads to a Marangoni recirculation some distance away from the contact line. The gel-COOH continues to deposit near the stagnation line, forming a volcano-like deposition profile. The black dashed line shows the focal plane at ≈10 $\mu$m above the substrate and the depth of field is a few micrometers using a 50× objective. Fluorescent particles and their motions are marked with red circles and arrows in the schematic. (b) Snapshots showing the motion of 1 $\mu$m fluorescent particles inside a 500 nL droplet of 3 wt % gel-COOH−12 wt % glycerol−0.75 wt % surfactant−water at two different times. The drop radius is about 1 mm and the height is around 300 $\mu$m. The red dashed lines show the edges of the stagnation zone. The arrows indicate the motion of fluorescent particles where one located below the focal plane moves toward the stagnation line and another on the focal plane moves toward the drop center. Different motions of the fluorescent particles on different $z$ planes indicate a Marangoni recirculation inside the drop as depicted in (a). (c) Velocity vectors inside the drop at $t \approx 20$ s. The scale bar represents 50 $\mu$m.

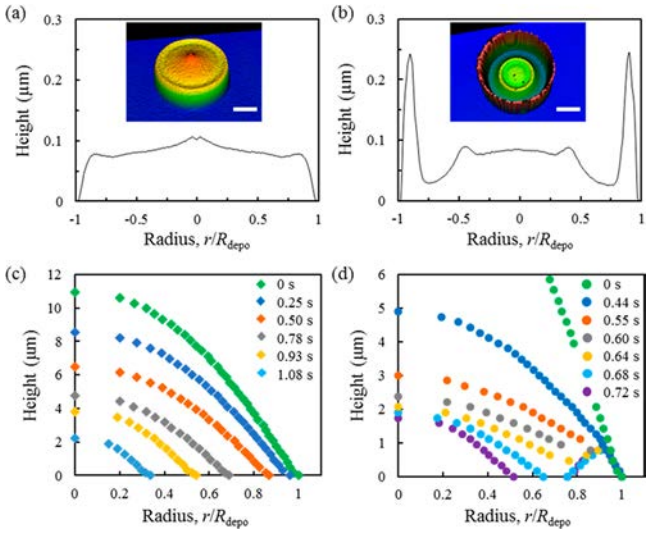


**Figure 9.** Deposition profiles of inkjet-printed polymer droplets containing 3 wt % gel-COOH−water (a) without and (b) with surfactant on a plasma-cleaned glass, with the inset showing the three-dimensional deposition profiles. The scale bar represents 50 $\mu$m. The instantaneous drop shapes (c) without and (d) with surfactant. The in-flight drop diameter is 60 $\mu$m at a relative humidity of 35%.

domelike to volcano-like at around 0.8 s and maintains a volcano-like profile until evaporation ends. An inflection point in drop profile is observed near the contact line at $t$ = 1.2 s, which is not seen for the case without surfactant.


DOI: 10.1021/acs.langmuir.9b01705
Langmuir XXXX, XXX, XXX−XXX

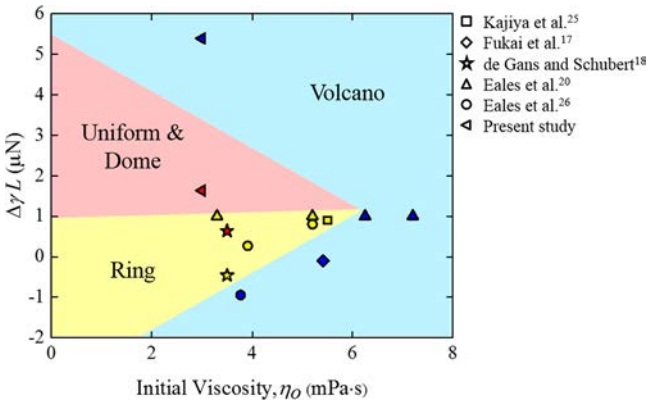


**Figure 10.** Final deposition profiles, including ring (yellow), uniform/dome (red), and volcano (blue) shapes, for different initial drop viscosities ($\eta_0$) and Marangoni forces ($\Delta\gamma L$) for an evaporating polymer drop with a pinned contact line.

Interferometry images shown in Figure 5b reveal the changes in fringe spacing over time. At $t$ = 0.4 s, the fringe spacing increases from the drop edge to the center, indicating a domelike profile. By analyzing interferometry images every 0.02 s, we found that the transition from domelike to volcano-like profile occurs right before 0.8 s. At $t$ = 0.8 s, a few fringes are concentrated near the contact line but no fringe at the drop center, indicating a near flat drop profile. At $t$ = 2.0 s, several fringes with decreasing spacing appear near the drop center, indicating a concave or volcano-like profile. After 2 s, the drop volume changes from 20% to 11.3% within 2 h. The smaller drop volume (or the faster evaporation rate) compared to the without surfactant case is mainly due to the surfactant-induced Marangoni recirculation, causing better mixing of remaining water and glycerol inside the drop. When the interferometry images of the same times in Figures 4b and 5b are compared, the instantaneous drop shape is found to be completely different after $t$ = 0.8 s by adding a small amount of surfactant.

Figure 6 shows the comparison of the normalized drop volumes, $V/V_0$, as a function of time with and without surfactant for droplets containing 3 wt % gel-COOH−12 wt % glycerol−85 wt % water on a plasma-cleaned glass substrate. The instantaneous drop volume is always smaller (or, in other words, the evaporation rate is higher) with surfactant until the drop volume reduces down to 20% at $t$ = 1.6 s when water is almost depleted. For both cases, the instantaneous drop volume deviates from the linear dependence with time as for a pure water drop with a pinned contact line on a hydrophilic surface.[43,44] This deviation is due to the presence of a less volatile component, glycerol, and the suppression of the evaporation-driven outward flow as a result of the accumulation of highly viscous gel-COOH and glycerol at the pinned contact line.

As the drop evaporates, the accumulation of gel-COOH, glycerol, and surfactant at the contact line induces a surface tension gradient along the drop surface. The drop center being rich in water has a higher surface tension compared to the drop edge rich in low surface tension components, which results in a Marangoni flow from the drop edge to the center. To compare the magnitudes of the Marangoni flows caused by gel-COOH, glycerol, and surfactant, individually, we calculated the Marangoni force for each component using $\Delta\gamma L$, where $L$ is the drop deposition radius which is about 85 × $10^{-6}$ m in our study and $\Delta\gamma$ is the maximum surface tension difference between the drop center and the edge. The values of $\Delta\gamma$ are estimated to be 44 mN/m for surfactant-induced Marangoni force (as the surfactant concentration increases from 0 to 5 wt %), 6 mN/m for glycerol-induced (as the glycerol concentration changes from 12 to 80 wt %), and 13 mN/m for gel-COOH-induced (as the gel-COOH concentration changes from 3 to 20 wt %), respectively. The corresponding Marangoni forces are 3.76 × $10^{-6}$ N for surfactant-driven, 0.53 × $10^{-6}$ N for glycerol-driven, and 1.11 × $10^{-6}$ N for gel-COOH-driven. This indicates that the surfactant-driven Marangoni flow dominates, and in the absence of surfactant, the Marangoni flow becomes much weaker. It is also important to note that the surface tension is very sensitive to a small amount of the surfactant (e.g., 0.75 wt %) but less sensitive to gel-COOH and glycerol such that the actual Marangoni forces due to gel-COOH and glycerol during the evaporation process are expected to be less than the above estimated values on the basis of the maximum possible Marangoni forces.

The schematics of the drop evaporation and polymer deposition processes of the gel-COOH−glycerol−water droplets without and with surfactant are illustrated in Figure 7. In the absence of surfactant as shown in Figure 7a, a strong evaporation-driven outward flow to replenish high evaporation flux at the pinned contact line drives gel-COOH and glycerol to the contact line region at an early stage of evaporation and creates a highly viscous region near the contact line. This highly viscous contact line region suppresses the evaporation-

**Table 2. Properties of the Ink Solutions Included in Figure 10**

| symbol | reference | component | $\Delta\gamma$ (N/m) | $L$ (m) | $\Delta\gamma L$ ($\mu$N) | $\eta_o$ (Pa·s) |
|---|---|---|---|---|---|---|
| □ | Kajiya et al.[25] | butanol−PDMA | 0.6 × $10^{-3}$ | 1.5 × $10^{-3}$ | 0.9 | 5.5 × $10^{-3}$ |
| ◇ | Fukai et al.[17] | xylene−PS | −2 × $10^{-3}$ | 5 × $10^{-5}$ | 0.1 | 5.416 × $10^{-3}$ |
| ☆ | De Gans and Schubert[18] | acetophenone−PS | 9.04 × $10^{-3}$ | 7 × $10^{-5}$ | 0.63 | 3.5 × $10^{-3}$ |
| | | ethyl acetate−PS | −6.61 × $10^{-3}$ | | −0.46 | |
| △ | Eales et al.[20] | MB−LEP Ink A | 8 × $10^{-3}$ | 12.5 × $10^{-5}$ | 1.0 | 3.3 × $10^{-3}$ |
| | | MB−LEP Ink B | | | | 5.2 × $10^{-3}$ |
| | | MB−LEP Ink C | | | | 7.2 × $10^{-3}$ |
| | | MB−LEP Ink G | | | | 6.25 × $10^{-3}$ |
| ○ | Eales et al.[26] | MB−LEP Ink A | 8 × $10^{-3}$ | 10 × $10^{-5}$ | 0.8 | 5.2 × $10^{-3}$ |
| | | MB−OX−LEP Ink C | 2.68 × $10^{-3}$ | | 0.27 | 3.912 × $10^{-3}$ |
| | | MB−AN−LEP Ink F | −9.48 × $10^{-3}$ | | −0.95 | 3.77 × $10^{-3}$ |
| ◁ | present study | gel-COOH−glycerol−water | 19.2 × $10^{-3}$ | 8.5 × $10^{-5}$ | 1.6 | 3.0 × $10^{-3}$ |
| | | gel-COOH−glycerol−water−Surfynol440 | 63.4 × $10^{-3}$ | | 5.4 | 3.0 × $10^{-3}$ |



DOI: 10.1021/acs.langmuir.9b01705
Langmuir XXXX, XXX, XXX−XXX

driven outward flow and forms a stagnation zone as gel-COOH and glycerol continue to accumulate. A weak Marangoni flow is induced from the drop edge to the center, and in conjunction with the suppressed evaporation-driven outward flow, the microflow inside the drop is not expected to be significant such that the solvent evaporates uniformly at the drop surface and results in a domelike deposition pattern.

In the presence of surfactant, as shown in Figure 7b, the accumulation of gel-COOH, glycerol, and surfactant to the contact line by the strong evaporation-driven outward flow creates a highly viscous stagnation zone near the drop edge that is similar to the case without surfactant. A strong Marangoni flow is induced from drop edge to center mainly because of the high surfactant concentration near the contact line. This strong Marangoni flow meets the stagnation zone near the drop edge and creates a recirculating flow inside the drop as shown in the third graph of Figure 7b. The combined recirculating flow with stagnation zone is believed to be responsible for the inflection point observed during drop evaporation in Figure 5a and the volcano-like deposition profile for gel-COOH−glycerol−water−surfactant drops.

To demonstrate the existence of a Marangoni recirculation with a stagnation zone at the contact line, the microflows inside a 500 nL drop consisting of 3 wt % gel-COOH−12 wt % glycerol−0.75 wt % surfactant−water was examined using fluorescent particles as flow tracers. A larger drop size was chosen to ensure enough fluorescent particles for flow visualization. As shown in Figure 8b, a stagnation zone near the drop contact line is formed within 20 s of evaporation because of the accumulation of gel-COOH and glycerol, and its width increases over time. A stagnation point of zero velocity appears at the edge of the stagnation zone and close to the drop surface. The microflow outside the stagnation zone is demonstrated using two fluorescent particles at two different $z$ planes. The particle located near the bottom of the drop moves toward the stagnation line and another on the focal plane about 10 $\mu$m above the substrate moves toward the drop center as shown in Figure 8b, indicating a Marangoni recirculation is set up some distance away from the contact line as illustrated by the streamlines in Figure 8a. To further verify the Marangoni recirculation, particle image velocimetry (PIV) algorithms were implemented to approximate the flow field inside the evaporating drop using open-source software, PIVlab (time-resolved digital particle image velocimetry tool for MATLAB).[45] Fluorescent images, every 0.2 s, were preprocessed through high-pass filtering and background noise subtraction algorithms to remove the out-of-focus particles. Velocity vectors shown in Figure 8c were obtained from consecutive frames at $t$ = 20 and 20.2 s based on two-dimensional cross-correlations with 48 × 48 pixels of 50% overlap. Marangoni recirculation with inward velocity on the focal plane of 10 $\mu$m above the substrate is clearly shown.

To understand the effect of surfactant in polymer drops with water-only solvent, deposition morphologies and instantaneous drop profiles are observed for an inkjet-printed 3 wt % gel-COOH−water droplet without and with surfactant. While a uniform deposition with a small center bump is obtained for the case without surfactant as shown in Figure 9a, a coffee-eye-like deposition with a central deposit and a thick ring at the contact line is observed in the presence of surfactant as shown in Figure 9b. With use of high-speed interferometry, continuous receding of the contact line is observed for the case without surfactant as shown in Figure 9c because of the lack of glycerol and hence no stagnation zone in the evaporating drop. In contrast, the contact line is initially pinned for the case with surfactant and an inflection point of the drop profile appears at $t$ = 0.64 s and around $r/R_{depo}$ = 0.76. And then, at $t$ = 0.68 s, the contact line starts to depin, leaving behind a ring deposition for the case with surfactant as shown in Figure 9d. Note that, in Figure 9c,d, only half of the drop is shown because of symmetry. The results show that the presence of surfactant reduces the drop surface tension and causes the depinning of contact line to be difficult. This observation is consistent with the model of Orejon et al.,[43] where the energy for depinning is found to be proportional to surface tension, and hence as the surfactant lowers the surface tension, the energy for depinning diminishes. The initial pinning of the contact line causes gel-COOH to accumulate at the drop edge, which further enhances pinning. As evaporation continues, the contact angle decreases. Once the contact angle becomes smaller than the critical receding contact angle, the contact line depins and a coffee-eye-like deposition is formed because of the Marangoni recirculation, which brings some gel-COOH to eventually deposit at the drop center as shown in Figure 9b.

Figure 10 summarizes the final deposition profiles from the literature and the present study, including ring, uniform, dome, and volcano shapes, for different initial drop viscosities ($\eta_0$) and Marangoni forces ($\Delta\gamma L$) for an evaporating polymer drop with a pinned contact line, representing two competing forces inside the drop. Different symbols in Figure 10 denote different studies and different colors indicate different deposition morphologies. The Marangoni force, $\Delta\gamma L$, can be induced by the gradient of solute, solvent, and surfactant along the drop surface and added together for a complex drop containing different causes of the Marangoni force. The properties of the ink solutions included in Figure 10 are summarized in Table 2. Positive and negative $\Delta\gamma L$ imply the inward and outward Marangoni flows, respectively. Initial drop viscosity, $\eta_0$, along the $x$-axis, is experimentally determined in the literature, except Eales et al.[26] for the bisolvent case. For the bisolvent case, viscosity is calculated using $\eta_0 = x_1\eta_1 + x_2\eta_2$, where $x_1$ and $x_2$ are the volumetric percentage and $\eta_1$ and $\eta_2$ are the viscocity of each solvent.[26,46,47] Change in viscosity by adding polymer in the bisolvent case is considered to be proportional to that of a single solvent.[20] A large Marangoni force with a high initial viscosity creates Marangoni recirculation because of the formation of stagnation zone at the contact line and is responsible for the volcano-shape deposition. However, a low initial drop viscosity and a reversed Marangoni force (i.e., negative $\Delta\gamma L$ value) are responsible for the ring-shape deposition. The uniform and dome shapes result from a low initial drop viscosity and a medium Marangoni force $\Delta\gamma L$. For the present study, the initial drop viscosity is high because of the presence of glycerol and polymer and a stagnation zone is formed. The Marangoni recirculation in the conjunction of the stagnation zone transitions the deposition from dome to volcano shape in the presence of surfactant, opposite the uniform deposition due to surfactant as observed by others.[30,48]

## CONCLUSION

In this study, the instantaneous evaporation process of inkjet-printed picoliter gelatin carboxyl drops containing glycerol and water is observed in real time using interferometry. In contrast to other drop deposition studies with surfactant, bisolvent



DOI: 10.1021/acs.langmuir.9b01705
Langmuir XXXX, XXX, XXX−XXX

gelatin drops with surfactants yield a volcano-shape deposition as a result of a strong Marangoni recirculation in conjunction with a stagnation zone near the contact line. Without surfactant, the suppressed evaporation-driven outward flow combined with a weak Marangoni flow results in a domelike deposition. For polymer drops in pure water, contact line depinning is observed without the stagnation zone for both with and without surfactant, and the presence of surfactant transitions the deposition morphology from uniform to coffee-eye-like. This study helps to understand the deposition dynamics of polymer drops to better control the deposition patterns for a broad range of polymer printing applications from OLEDs to biomedical implants.

## AUTHOR INFORMATION


### Corresponding Author

*Tel.: (215)895-1373. Fax: (215)895-1478. E-mail: ysun@coe.drexel.edu (Y.S.).

### ORCID

Ying Sun: 0000-0003-4748-376X


### Notes

The authors declare no competing financial interest.

## ACKNOWLEDGMENTS

Support for this work was provided by the U.S. National Science Foundation under Grant Nos. CMMI-1401438 and CBET-1705745.

## REFERENCES


(1) Soltman, D.; Subramanian, V. Inkjet-Printed Line Morphologies and Temperature Control of the Coffee Ring Effect. *Langmuir* **2008**, *24* (5), 2224−2231.

(2) Hoth, C. N.; Schilinsky, P.; Choulis, S. A.; Brabec, C. J. Printing Highly Efficient Organic Solar Cells. *Nano Lett.* **2008**, *8* (9), 2806−2813.

(3) Daly, R.; Harrington, T. S.; Martin, G. D.; Hutchings, I. M. Inkjet Printing for Pharmaceutics - A Review of Research and Manufacturing. *Int. J. Pharm.* **2015**, *494* (2), 554−567.

(4) Langer, R.; Peppas, N. A. Advances in Biomaterials, Drug Delivery, and Bionanotechnology. *AIChE J.* **2003**, *49* (12), 2990−3006.

(5) Langer, R. Biomaterials in Drug Delivery and Tissue Engineering: One Laboratory's Experience. *Acc. Chem. Res.* **2000**, *33* (2), 94−101.

(6) Jungst, T.; Smolan, W.; Schacht, K.; Scheibel, T.; Groll, J. Strategies and Molecular Design Criteria for 3D Printable Hydrogels. *Chem. Rev.* **2016**, *116* (3), 1496−1539.

(7) Melchels, F. P. W.; Domingos, M. A. N.; Klein, T. J.; Malda, J.; Bartolo, P. J.; Hutmacher, D. W. Additive Manufacturing of Tissues and Organs. *Prog. Polym. Sci.* **2012**, *37* (8), 1079−1104.

(8) Roth, E. A.; Xu, T.; Das, M.; Gregory, C.; Hickman, J. J.; Boland, T. Inkjet Printing for High-Throughput Cell Patterning. *Biomaterials* **2004**, *25* (17), 3707−3715.

(9) Wilson, W. C.; Boland, T. Cell and Organ Printing 1: Protein and Cell Printers. *Anat. Rec.* **2003**, *272A* (2), 491−496.

(10) Baldwin, K. A.; Granjard, M.; Willmer, D. I.; Sefiane, K.; Fairhurst, D. J. Drying and Deposition of Poly(Ethylene Oxide) Droplets Determined by Péclet Number. *Soft Matter* **2011**, *7* (17), 7819.

(11) Murphy, S. V.; Atala, A. 3D Bioprinting of Tissues and Organs. *Nat. Biotechnol.* **2014**, *32* (8), 773−785.

(12) Ambekar, R. S.; Kandasubramanian, B. Progress in the Advancement of Porous Biopolymer Scaffold: Tissue Engineering Application. *Ind. Eng. Chem. Res.* **2019**, *58* (16), 6163−6194.

(13) Hewes, S.; Wong, A. D.; Searson, P. C. Bioprinting Microvessels Using an Inkjet Printer. *Bioprinting* **2017**, *7*, 14−18.

(14) Mouser, V. H. M.; Levato, R.; Bonassar, L. J.; D'Lima, D. D.; Grande, D. A.; Klein, T. J.; Saris, D. B. F.; Zenobi-Wong, M.; Gawlitta, D.; Malda, J. Three-Dimensional Bioprinting and Its Potential in the Field of Articular Cartilage Regeneration. *Cartilage* **2017**, *8* (4), 327−340.

(15) Kajiya, T.; Kaneko, D.; Doi, M. Dynamical Visualization of "Coffee Stain Phenomenon" in Droplets of Polymer Solution via Fluorescent Microscopy. *Langmuir* **2008**, *24* (21), 12369−12374.

(16) Kim, J. H.; Park, S. B.; Kim, J. H.; Zin, W. C. Polymer Transports inside Evaporating Water Droplets at Various Substrate Temperatures. *J. Phys. Chem. C* **2011**, *115* (31), 15375−15383.

(17) Fukai, J.; Ishizuka, H.; Sakai, Y.; Kaneda, M.; Morita, M.; Takahara, A. Effects of Droplet Size and Solute Concentration on Drying Process of Polymer Solution Droplets Deposited on Homogeneous Surfaces. *Int. J. Heat Mass Transfer* **2006**, *49* (19−20), 3561−3567.

(18) De Gans, B. J.; Schubert, U. S. Inkjet Printing of Well-Defined Polymer Dots and Arrays. *Langmuir* **2004**, *20* (18), 7789−7793.

(19) Cho, H. R.; Park, W. I.; Song, Y. S.; Jung, J.; Choe, A.; Ko, H.; Byun, M. Spontaneous Capillary Breakup of Suspended Gradient Polymer Stripes into Spatially Ordered Dot Arrays. *Appl. Surf. Sci.* **2019**, *475*, 1003−1009.

(20) Eales, A. D.; Routh, A. F.; Dartnell, N.; Simon, G. Evaporation of Pinned Droplets Containing Polymer − An Examination of the Important Groups Controlling Final Shape. *AIChE J.* **2015**, *61* (5), 1759−1767.

(21) Okuzono, T.; Kobayashi, M.; Doi, M. Final Shape of a Drying Thin Film. *Phys. Rev. E* **2009**, *80* (2), 021603.

(22) Ozawa, K.; Nishitani, E.; Doi, M. Modeling of the Drying Process of Liquid Droplet to Form Thin Film. *Japanese J. Appl. Phys., Part 1 Regul. Pap. Short Notes Rev. Pap.* **2005**, *44* (6A), 4229−4234.

(23) Cui, L.; Zhang, J.; Zhang, X.; Huang, L.; Wang, Z.; Li, Y.; Gao, H.; Zhu, S.; Wang, T.; Yang, B. Suppression of the Coffee Ring Effect by Hydrosoluble Polymer Additives. *ACS Appl. Mater. Interfaces* **2012**, *4*, 2775−2780.

(24) Seo, C.; Jang, D.; Chae, J.; Shin, S. Altering the Coffee-Ring Effect by Adding a Surfactant-like Viscous Polymer Solution. *Sci. Rep.* **2017**, *7* (1), 500.

(25) Kajiya, T.; Monteux, C.; Narita, T.; Lequeux, F.; Doi, M. Contact-Line Recession Leaving a Macroscopic Polymer Film in the Drying Droplets of Water-Poly(N, N-Dimethylacrylamide) (PDMA) Solution. *Langmuir* **2009**, *25* (12), 6934−6939.

(26) Eales, A. D.; Dartnell, N.; Goddard, S.; Routh, A. F. Thin Binary Liquid Droplets, Containing Polymer: An Investigation of the Parameters Controlling Film Shape. *J. Fluid Mech.* **2016**, *794* (2011), 200−232.

(27) Babatunde, P. O.; Hong, W. J.; Nakaso, K.; Fukai, J. Effect of Solute- and Solvent-Derived Marangoni Flows on the Shape of Polymer Films Formed from Drying Droplets. *AIChE J.* **2013**, *59* (3), 699−702.

(28) Tekin, E.; Smith, P. J.; Hoeppener, S.; van den Berg, A. M. J.; Susha, A. S.; Rogach, A. L.; Feldmann, J.; Schubert, U. S. Inkjet Printing of Luminescent CdTe Nanocrystal − Polymer Composites. *Adv. Funct. Mater.* **2007**, *17*, 23−28.

(29) Kim, H.; Boulogne, F.; Um, E.; Jacobi, I.; Button, E.; Stone, H. A. Controlled Uniform Coating from the Interplay of Marangoni Flows and Surface-Adsorbed Macromolecules. *Phys. Rev. Lett.* **2016**, *116* (12), 124501.

(30) Kajiya, T.; Kobayashi, W.; Okuzono, T.; Doi, M. Controlling the Drying and Film Formation Processes of Polymer Solution Droplets with Addition of Small Amount of Surfactants. *J. Phys. Chem. B* **2009**, *113* (47), 15460−15466.

(31) Thokchom, A. K.; Shin, S. Dynamical Clustering and Band Formation of Particles in a Marangoni Vortexing Droplet. *Langmuir* **2019**, *35*, 8977−8983.

(32) Zhu, Z.; Ning, H.; Cai, W.; Wei, J.; Zhou, S.; Yao, R.; Lu, X.; Zhang, J.; Zhou, Z.; Peng, J. Morphology Modulation of Direct Inkjet




DOI: 10.1021/acs.langmuir.9b01705
*Langmuir* XXXX, XXX, XXX−XXX

Printing by Incorporating Polymers and Surfactants into a Sol-Gel Ink System. *Langmuir* **2018**, *34* (22), 6413−6419.
(33) de Ruiter, J.; Mugele, F.; van den Ende, D. Air Cushioning in Droplet Impact. I. Dynamics of Thin Films Studied by Dual Wavelength Reflection Interference Microscopy. *Phys. Fluids* **2015**, *27* (1), 012104.
(34) Van Der Veen, R. C. A.; Tran, T.; Lohse, D.; Sun, C. Direct Measurements of Air Layer Profiles under Impacting Droplets Using High-Speed Color Interferometry. *Phys. Rev. E* **2012**, *85* (2), 026315.
(35) https://www.mathworks.com/help/matlab/ref/spline.html, accessed on August 23, 2019.
(36) Kern, W. F.; Bland, J. R. *Theorem of Pappus in Solid Mensuration with Proofs*, 2nd ed.; Wiley: New York, 1948.
(37) EVONIK. Surfynol 440 Surfactant; 2017.
(38) Lide, D. R. *CRC Handbook of Data on Organic Compounds*, 3rd ed.; CRC Press: Boca Raton, FL, 1994.
(39) Cengel, Y. A.; Boles, M. A. *Thermodynamics: An Engineering Approach*, 8th ed.; McGraw-Hill: Boston, 2014.
(40) Kim, D.-O.; Pack, M.; Rokoni, A.; Kaneelil, P.; Sun, Y. The Effect of Particle Wettability on the Stick-Slip Motion of the Contact Line. *Soft Matter* **2018**, *14* (47), 9599−9608.
(41) Hu, H.; Larson, R. G. Evaporation of a Sessile Droplet on a Substrate. *J. Phys. Chem. B* **2002**, *106* (6), 1334−1344.
(42) Kim, D.-O.; Pack, M.; Hu, H.; Kim, H.; Sun, Y. Deposition of Colloidal Drops Containing Ellipsoidal Particles: Competition between Capillary and Hydrodynamic Forces. *Langmuir* **2016**, *32*, 11899−11906.
(43) Orejon, D.; Sefiane, K.; Shanahan, M. E. R. Stick-Slip of Evaporating Droplets: Substrate Hydrophobicity and Nanoparticle Concentration. *Langmuir* **2011**, *27* (21), 12834−12843.
(44) Deegan, R. D.; Bakajin, O.; Dupont, T. F.; Huber, G.; Nagel, S. R.; Witten, T. A. Contact Line Deposits in an Evaporating Drop. *Phys. Rev. E: Stat. Phys., Plasmas, Fluids, Relat. Interdiscip. Top.* **2000**, *62* (1), 756−765.
(45) Thielicke, W.; Stamhuis, E. J. PIVlab − Towards User-Friendly, Affordable and Accurate Digital Particle Image Velocimetry in MATLAB. *J. Open Res. Software* **2014**, *2* (1), e30.
(46) Weng, W. L. Densities and Viscosities for Binary Mixtures of Anisole with 2-Butanol, 2-Methyl-1-Propanol, and 2-Methyl-2-Propanol. *J. Chem. Eng. Data* **1999**, *44* (4), 788−791.
(47) Dean, J. A. *Lange's Handbook of Chemistry*, 10th ed.; McGraw-Hill, 1992.
(48) Seo, C.; Jang, D.; Chae, J.; Shin, S. Altering the Coffee-Ring Effect by Adding a Surfactant-like Viscous Polymer Solution. *Sci. Rep.* **2017**, *7* (1), 500.



DOI: 10.1021/acs.langmuir.9b01705
*Langmuir* XXXX, XXX, XXX−XXX